

ES-Merging: Biological MLLM Merging via Embedding Space Signals

Wonbin Lee*¹ Dongki Kim*¹ Sung Ju Hwang^{1,2}

¹KAIST ²DeepAuto.ai

{smilelwb01, cleverki, sungju.hwang}@kaist.ac.kr

Abstract

Biological multimodal large language models (MLLMs) have emerged as powerful foundation models for scientific discovery. However, existing models are specialized to a single modality, limiting their ability to solve inherently cross-modal scientific problems. While model merging is an efficient method to combine the different modalities into a unified MLLM, existing methods rely on input-agnostic parameter space heuristics that fail to faithfully capture modality specialization. To overcome this limitation, we propose a representation-aware merging framework that estimates merging coefficients from embedding space signals. We first design a probe input that consists of different modality tokens and forward it through each specialized MLLM to obtain layer-wise embedding responses that reflect modality-specific representation changes. We then estimate complementary merging coefficients at two granularities from the embedding space: layer-wise coefficients from coarse-grained signals and element-wise coefficients from fine-grained signals, which are jointly combined for robust coefficient estimation. Experiments on interactive effect prediction benchmarks show that our method outperforms existing merging methods and even surpasses task-specific fine-tuned models, establishing that embedding space signals provide a principled and effective foundation for cross-modal MLLM merging.

1 Introduction

Multimodal Large Language Models (MLLMs) have been emerging as crucial foundational models for scientific discovery, extending their perception to diverse biological modalities across molecules (Park et al., 2024; Kim et al., 2025), proteins (Abdine et al., 2024; Fei et al., 2025), and

cells (Fang et al., 2025b; Rizvi et al., 2025). Despite their impressive progress within each modality, many scientific problems of interest are cross-modal, requiring to understand the interactive effects such as protein-ligand interactions or drug effectiveness to cell types. However, existing biological MLLMs are specialized to a single modality, resulting in limited intersectional knowledge and unreliable cross-modal reasoning.

Building a unified model by jointly training on different modalities is a straightforward approach to upskill cross-modal understanding. However, it is impractical and time-consuming since constructing curated cross-modal instruction datasets in the scientific domain typically requires intensive labor and highly specific expertise to elaborate the underlying principles of complex interactions. As an alternative, model merging has gained attention by efficiently combining parameters of multiple specialized models. To retain their task-specific knowledge, existing methods (Yadav et al., 2023; Huang et al., 2024; Du et al., 2024) exploit parameter space signals, such as magnitudes, signs, and directions, heuristically assigning merging coefficients. However, parameter space heuristics are input-agnostic and therefore provide only weak, indirect proxies for modality-specific adaptation. Such input-blindness makes it difficult to isolate meaningful cross-modal interactions, failing to accurately combine these adaptations and severely degrading cross-modal merging.

Our main observation is that the input-aware embedding space contains the modality-specific information. As shown in Fig. 1, when molecular tokens are processed by different MLLMs, the hidden representations form clearly different embedding distributions. In particular, the molecule-specific LLM induces a more distinct distribution due to its modality-specific understanding. Further, we measure the embedding distribution distance between the base LLM and each specialized MLLM

* denotes Equal Contribution

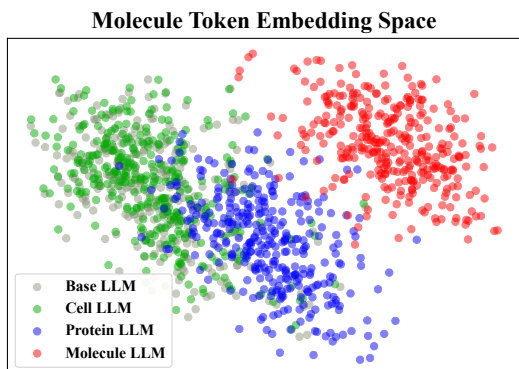


Figure 1: Molecule token embedding visualization of the last transformer block for the base LLM and each specialized LLM.

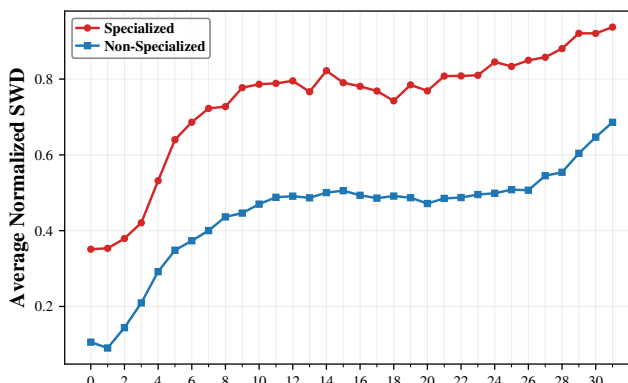


Figure 2: Layer-wise embedding distribution distance under specialized and non-specialized tokens using sliced Wasserstein distances (SWD) (Bonneel et al., 2015).

under specialized and non-specialized token inputs. Fig. 2 shows that specialized inputs consistently produce larger embedding distribution distance than non-specialized inputs, suggesting that the embedding responses faithfully reflect modality-specific adaptation when the input matches the model’s specialization. This observation motivates our central design principle: rather than relying solely on heuristic parameter space signals, we estimate merging coefficients based on the layer-wise embedding space signals.

Motivated by this observation, we propose an embedding-signal-based MLLM merging (**ES-Merging**), a novel framework that moves the model merging paradigm from parameter space signals to embedding space signals. Our intuition is that the modality specialization of an MLLM can be measured by the differences in the embedding space between the base LLM and the MLLM as shown in Fig. 1. To this end, we first design a probe input containing multimodal tokens of different modalities. By forwarding this input through each MLLM and the base LLM, we obtain layer-wise embeddings that reflect modality-specific representation changes across layers.

Based on these embeddings, we propose to compute merging coefficients at two complementary granularities: layer-wise and element-wise. In the layer-wise manner, we compute a layer-level importance score by identifying layers where the embedding distributional shift grows the most, capturing coarse-grained specialization. In the element-wise manner, we estimate fine-grained importance by identifying parameters that most influence the representation shift. We then combine the coarse layer importance and fine element importance to produce final merging coefficients, which are used to fuse specialized models into a single unified MLLM.

This design enables more robust and calibrated coefficient estimation by combining layer-level specialization with parameter-level sensitivity.

We validate the effectiveness of ES-Merging on interactive effect prediction tasks over diverse biological modalities by merging three different specialized MLLMs into a single unified model. Experimental results show that ES-Merging outperforms not only other model merging methods but also the task-specific fine-tuned models, empirically confirming our representation-aware merging framework is crucial to obtain the salient modality-specific signals. Further analyses show the effectiveness of our components: combining layer- and element-wise merging coefficients best performs compared to using only one, highlighting the necessity of integrating complementary specialization signals at different granularities.

2 Related Work

MLLMs for Scientific Discovery Large language models (LLMs) (Touvron et al., 2023; Grattafiori et al., 2024; OpenAI, 2024a,b; Comanici et al., 2025) are increasingly being extended to scientific discovery through multimodal large language models (MLLMs) that incorporate diverse biological modalities, including molecules (Wang et al., 2025b), proteins (Xiao et al., 2025), and cells (Dip et al., 2025). In the protein domain, prior works have modeled amino-acid sequences (Xu et al., 2023; Pei et al., 2023) or jointly with structures (Guo et al., 2023; Abdine et al., 2024; Wang et al., 2024a; Xiao et al., 2024; Wang et al., 2025a; Fei et al., 2025). Single cell LLMs learn the scRNA-seq representations (Fang et al., 2025a; Kharouiche et al., 2025; Fang et al., 2025b) or further incorporate histology information (Li et al., 2025; Chen et al., 2025). On the other hand,

molecular LLMs have been built on 1D string representations such as SMILES (Weininger, 1988) and SELFIES (Krenn et al., 2020) (Chithrananda et al., 2020; Edwards et al., 2022), 2D molecular graphs (Liu et al., 2023; Fang et al., 2023; Cao et al., 2023; Yu et al., 2024; Park et al., 2024), 3D structures (Li et al., 2024; Guo et al., 2024), and joint 2D-3D representations (Kim et al., 2025). Despite this progress, biological MLLMs are limited to a single modality, hindering their ability to solve cross-modal scientific problems.

Model Merging Model merging aims to fuse knowledge from multiple specialist models with minimal additional data or training by combining them directly in parameter space. Existing methods mainly leverage the parameter space signals to guide merging. Magnitude-based methods include Task Arithmetic (Ilharco et al., 2022), Consensus Merging (Wang et al., 2024b), and PCB-Merging (Du et al., 2024); sign-based methods include TIES-Merging (Yadav et al., 2023) and EMR-Merging (Huang et al., 2024); and LS-Merge (Soro et al., 2026) performs merging in a learned latent space over parameters. Beyond such static merging, test-time adaptation methods dynamically adjust coefficients using unlabeled test data, as in AdaMerging (Yang et al., 2023) and Twin-Merging (Lu et al., 2024). However, these methods still rely on parameter space signals, which are not well suited to capturing semantic discrepancies across heterogeneous modalities. We instead propose an embedding space merging framework for MLLMs that derives merging coefficients from modality-aware representation signals.

3 Preliminary

We begin by formally describing MLLMs, then formulating the model merging with LoRA.

Multimodal Large Language Model MLLMs operate beyond the textual space by taking modality token embeddings with text tokens. Concretely, let $\mathcal{M} = \{m_1, \dots, m_K\}$ denote a set of modalities. For each modality m_i , a modality-specific encoder f_{m_i} projects the raw modality input \mathbf{x}_{m_i} to a sequence of modality tokens: $\mathbf{H}_{m_i} = f_{m_i}(\mathbf{x}_{m_i})$. Then, an MLLM generates textual output \mathbf{y} by taking the concatenated textual and modality tokens:

$$\mathbf{y} = g(\mathbf{H}^0), \text{ where } \mathbf{H}^0 = [\mathbf{H}_{\text{text}}; \mathbf{H}_{m_i}; \dots].$$

In this view, the core interface of an MLLM

is the token-based embeddings: raw modality inputs are first mapped into sequences of vectors that are compatible with the LLM’s embedding dimension, and then processed together by a single transformer.

LoRA Merging In the MLLM setting, modality specialization is often implemented as a parameter efficient tuning with LoRA (Hu et al., 2022). Therefore, our merging methods are based on merging LoRA parameters via weighted summation. Specifically, let θ_{m_i} denote the LoRA parameter of an MLLM specialized to modality m_i . We index the parameters by layer and weight element: $\theta_{m_i}^{l,n}$ denotes the n -th weight in the l -th layer of the modality-specific model for m_i . Then, the LoRA merging is formalized as follows:

$$\theta_{\text{uni}}^{l,n} \leftarrow \sum_{m_i \in \mathcal{M}} \lambda_{m_i}^{l,n} \theta_{m_i}^{l,n}. \quad (1)$$

Under this formulation, the main challenge is to estimate appropriate merging coefficients $\lambda_{m_i}^{l,n}$ that determine how strongly each modality-specific LoRA parameter contributes to the modality understanding. Our method addresses this coefficient estimation problem by deriving $\lambda_{m_i}^{l,n}$ from embedding space signals rather than parameter space statistics.

4 ES-Merging

We present Embedding-Signal-based MLLM Merging (ES-Merging), a representation-aware framework for merging modality-specialized MLLMs based on embedding space signals. Specifically, ES-Merging constructs probe inputs to elicit representational differences across models, and converts these embedding space discrepancies into layer-wise and element-wise merging coefficients.

4.1 Probe Input

As discussed in Section 3, we view the projected modality tokens as the core interface of the LLM backbones. In other words, once a raw modality input is mapped into the shared embedding space, the modality-specific knowledge of an MLLM is reflected in how the backbone interprets and transforms these token embeddings across layers. From this perspective, understanding modality specialization reduces to analyzing the layer-wise transformation of modality tokens in representation space. Motivated by this view, we design probe inputs that explicitly expose token embeddings of different modalities, so that we can compare how the

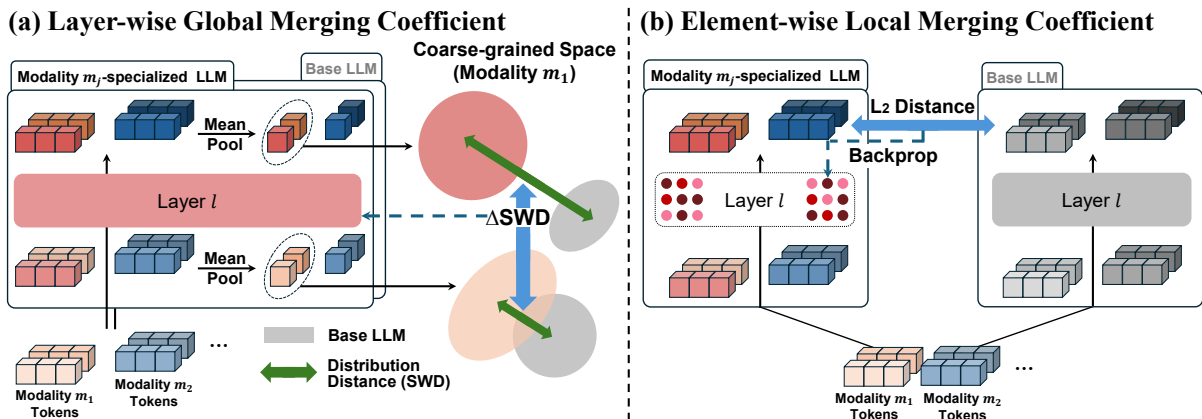


Figure 3: Overview of ES-Merging. (A) Layer-wise global merging coefficients are computed from the coarse-grained embedding signals, which are the layer-wise differences of distribution distances between mean pooled representations of the base LLM and a specialized MLLM. (B) Element-wise local merging coefficients are assigned based on the fine-grained embedding signals by computing the gradients from the embedding-wise distances.

base LLM and each modality-specialized MLLM process the same modality embeddings.

Specifically, for each modality m_i , we collect a set of raw inputs $\{\mathbf{x}_{m_i}^{(k)}\}_{k=1}^K$ from corresponding datasets and transform them via the modality-specific encoder f_{m_i} into the modality token embeddings $\{\mathbf{H}_{m_i}^{(k)}\}_{k=1}^K$, where $\mathbf{H}_{m_i}^{(k)} = f_{m_i}(\mathbf{x}_{m_i}^{(k)})$. Using these embeddings, we then build the probe input by concatenating a short textual prefix with all modality token blocks:

$$\mathbf{H}_{\text{probe}}^{0,(k)} = [\mathbf{H}_{\text{text},m_1}; \mathbf{H}_{m_1}^{(k)}; \mathbf{H}_{\text{text},m_2}; \mathbf{H}_{m_2}^{(k)}; \dots],$$

where $\mathbf{H}_{\text{text},m_i}$ denotes the text-prefix embeddings associated with modality m_i (e.g., the modality identifier or name). In the biological setting, the modality set \mathcal{M} typically consists of $\{\text{molecule, protein, cell}\}$, and the resulting probe input is illustrated in Fig. 4. By forwarding each probe input through the base LLM and each MLLM specialized to modality m_j , we obtain layer-wise embeddings by extracting the modality m_i tokens, denoted as $\mathbf{H}_{m_i \rightarrow \text{base}}^{l,(k)}$ and $\mathbf{H}_{m_i \rightarrow \theta_{m_j}}^{l,(k)}$ in $\mathbb{R}^{T_{m_i} \times d}$, where l denotes the layer index and T_{m_i} denotes the number of modality- m_i tokens.

These layer-wise representations serve as the foundation for our subsequent merging coefficient estimation. We regard the embedding discrepancy between the base LLM and each modality-specialized MLLM as an embedding space signal that reflects the degree of the modality specialization. We then leverage this signal at two complementary levels: globally across layers to estimate which layers contribute more to specialization, and locally within each layer to identify which param-



Figure 4: Prompt template of the probe input.

ter elements are more strongly associated with the specialized transformation.

4.2 Layer-wise Global Merging Coefficient

To capture global modality specialization, we compute a layer-wise global merging coefficient from coarse-grained embedding signals (Fig. 3 (a)).

Coarse-grained Embedding Signal We first summarize the modality-specific embeddings into a coarse-grained representation by averaging token-level embeddings, obtaining $\hat{\mathbf{h}}_{m_i \rightarrow \text{base}}^{l,(k)} \in \mathbb{R}^d$ for the base model and $\hat{\mathbf{h}}_{m_i \rightarrow \theta_{m_j}}^{l,(k)} \in \mathbb{R}^d$ for a specialized model θ_{m_j} . By collecting these coarse-grained embeddings over different K probe inputs, we obtain two layer-wise embedding sets, $\mathcal{H}_{m_i \rightarrow \text{base}}^l \in \mathbb{R}^{K \times d}$ and $\mathcal{H}_{m_i \rightarrow \theta_{m_j}}^l \in \mathbb{R}^{K \times d}$, which represent how the base and specialized models process modality- m_i inputs at layer l . We then quantify their representational gap using the embedding distribution distance with sliced Wasserstein distance (SWD) (Bonnel et al., 2015):

$$\text{SWD}_{m_i \rightarrow \theta_{m_j}}^l = \text{SWD}\left(\mathcal{H}_{m_i \rightarrow \text{base}}^l, \mathcal{H}_{m_i \rightarrow \theta_{m_j}}^l\right).$$

A larger value indicates that θ_{m_j} induces a stronger layer-wise shift from the base model when processing modality- m_i tokens.

Layer-wise Importance Estimation While $\text{SWD}_{m_i \rightarrow \theta_{m_j}}^l$ measures the cumulative differences up to layer l , we are particularly interested in how much new modality-specific transformation is introduced at each layer. We therefore compute the layer-wise change:

$$d_{m_i \rightarrow \theta_{m_j}}^l = \text{SWD}_{m_i \rightarrow \theta_{m_j}}^l - \text{SWD}_{m_i \rightarrow \theta_{m_j}}^{l-1}.$$

If $d_{m_i \rightarrow \theta_{m_j}}^l$ is large, the corresponding layer of model θ_{m_j} contributes more strongly to modality m_i -specific processing. Since the magnitude of these changes can vary across models, we normalize them over layers using Z-score normalization, obtaining $\hat{d}_{m_i \rightarrow \theta_{m_j}}^l$. We aggregate the normalized changes over all input modalities to obtain the layer-wise importance score of model θ_{m_j} :

$$s_{\theta_{m_j}}^l = \sum_{m_i \in \mathcal{M}} \hat{d}_{m_i \rightarrow \theta_{m_j}}^l.$$

Layer-wise Global Coefficient Finally, we convert the layer-wise importance scores into merging coefficients by applying a softmax across models:

$$\alpha_{m_j}^l = \frac{\exp(s_{\theta_{m_j}}^l / \tau)}{\sum_{m \in \mathcal{M}} \exp(s_{\theta_m}^l / \tau)}. \quad (2)$$

As a result, a specialized MLLM receives a larger coefficient at layers where it contributes more strongly to coarse-grained representational changes over different modality inputs.

4.3 Element-wise Local Merging Coefficient

While the layer-wise global coefficient captures modality importance at the transformer-layer level, it assigns a uniform merging weight to all parameters within the same layer. To address this limitation, we further introduce an element-wise local merging coefficient derived from fine-grained embedding signals (Fig. 3 (b)).

Fine-grained Embedding Signals To measure the fine-grained signals from embeddings, we first measure the distances of each embedding between the base model and a specialized model θ_{m_j} , instead of using the coarse-grained representations:

$$r_{m_i \rightarrow \theta_{m_j}}^{l,(k)} = \left\| \mathbf{H}_{m_i \rightarrow \text{base}}^{l,(k)} - \mathbf{H}_{m_i \rightarrow \theta_{m_j}}^{l,(k)} \right\|_F,$$

where F denotes the Frobenius norm, which is analogous to the Euclidean L_2 norm for vectors. This distance measures how differently the specialized model θ_{m_j} processes modality- m_i inputs relative to the base model at layer l in a fine-grained manner.

Element-wise Importance Estimation We then estimate the importance of each parameter element by measuring how sensitive this distance is to that element. Specifically, for the n -th parameter element in layer l , we accumulate the absolute gradient magnitude over all modalities and probe inputs:

$$s_{\theta_{m_j}}^{l,n} = \sum_{m_i \in \mathcal{M}} \sum_{k=1}^K \left| \frac{\partial r_{m_i \rightarrow \theta_{m_j}}^{l,(k)}}{\partial \theta_{m_j}^{l,n}} \right|.$$

A larger score indicates that the parameter element is more sensitive to the modality-specific differences between the base and specialized models. Because the raw scores can vary across layers and parameters, we normalize them within each layer using Z-score normalization, yielding $\hat{s}_{\theta_{m_j}}^{l,n}$.

Element-wise Local Coefficient We convert the normalized scores into element-wise merging coefficients by applying the softmax function:

$$\beta_{m_j}^{l,n} = \frac{\exp(\hat{s}_{\theta_{m_j}}^{l,n} / \tau)}{\sum_{m \in \mathcal{M}} \exp(\hat{s}_{\theta_m}^{l,n} / \tau)}. \quad (3)$$

Resulting element-wise merging coefficients selectively assign each parameter element according to their fine-grained sensitivities.

4.4 Integrating Layer- and Element-wise Merging Coefficients

The coarse-grained layer-wise coefficient $\alpha_{m_i}^l$ and the fine-grained element-wise coefficient $\beta_{m_i}^{l,n}$ each capture modality-specific importance at different levels of granularity. We combine them into a single coefficient by multiplying the layer-wise coefficient and the element-wise coefficient and renormalizing across modalities:

$$\lambda_{m_i}^{l,n} = \frac{\alpha_{m_i}^l \cdot \beta_{m_i}^{l,n}}{\sum_{m \in \mathcal{M}} \alpha_m^l \cdot \beta_m^{l,n}}. \quad (4)$$

The final parameters of the merged model are computed by Eq. 1. By integrating different coefficient types from different granularities of embedding signals, ES-Merging enables calibrated merging coefficients that preserve complementary modality expertise more faithfully, enabling robust cross-modal knowledge composition.

5 Experimental Results

5.1 Experimental Setup

Implementation Details For merging, we leverage the state-of-the-art MLLMs specialized to

	Molecule-Protein Interaction								Molecule-Cell Interaction					
	BindingDB		BioSNAP		Human		Avg.		DrugComb		GDSC2		Avg.	
	Acc.	F1	Acc.	F1	Acc.	F1	Acc.	F1	Acc.	F1	Acc.	F1	Acc.	F1
<i>Base LLM and Specialized MLLMs</i>														
LLaMA-3.1-8B-Instruct	51.9	51.7	61.5	60.2	59.0	58.8	57.5	56.9	73.7	77.1	84.8	85.7	79.3	81.4
Mol-LLaMA (Kim et al., 2025)	55.8	54.7	<u>66.5</u>	64.0	<u>61.5</u>	<u>61.4</u>	61.2	60.0	64.1	80.4	55.2	82.3	59.7	81.4
Prot2Text-V2 (Fei et al., 2025)	59.2	59.2	55.3	54.1	47.2	47.2	53.9	53.5	65.6	78.4	59.7	67.0	62.6	72.7
Cell-o1 (Fang et al., 2025b)	53.5	53.1	59.3	59.8	49.1	48.5	54.0	53.8	76.3	77.2	85.9	86.0	81.1	81.6
<i>Merging Methods</i>														
Avg. Merging	65.3	64.9	66.4	66.5	60.9	60.9	64.2	64.1	72.5	74.6	85.4	87.9	78.9	81.2
TIES-Merging (Yadav et al., 2023)	60.8	60.8	62.7	61.6	58.6	58.6	60.7	60.3	74.7	77.0	85.9	87.1	80.3	82.1
EMR-Merging (Huang et al., 2024)	<u>64.7</u>	<u>64.2</u>	66.3	<u>66.9</u>	60.4	60.4	<u>63.8</u>	<u>63.8</u>	45.2	71.5	93.4	93.3	69.3	82.4
AdaMerging (Yang et al., 2023)	52.3	51.6	64.3	62.0	60.0	60.2	58.9	57.9	48.0	36.9	46.5	38.8	47.2	37.8
PCB-Merging (Du et al., 2024)	55.1	55.1	60.3	58.8	58.6	58.4	58.0	57.4	77.3	78.7	86.0	86.1	81.7	82.4
Consensus Merging (Wang et al., 2024b)	59.2	59.3	62.1	61.0	59.2	59.1	60.2	59.8	76.0	78.4	84.3	85.8	80.2	82.1
LS-Merge (Soro et al., 2026)	52.3	52.1	61.8	60.6	58.8	58.5	57.7	57.1	79.1	79.0	83.5	83.3	81.3	81.1
Avg. Merging + FT	60.5	59.7	55.8	55.9	57.2	57.3	57.8	57.6	81.1	80.8	94.0	93.9	87.5	87.4
ES-Merging (Ours)	66.0	65.3	69.1	68.4	62.0	61.9	65.7	65.2	<u>80.7</u>	<u>80.2</u>	94.1	94.0	<u>87.4</u>	<u>87.1</u>

Table 1: Performance comparison of ES-Merging with the base LLM with and without task-specific fine-tuning, specialized MLLMs, and merging methods on the instance-varying interaction prediction tasks. We report accuracy and macro-F1 across each subset. **Bold** and underline indicate the best and second best performances, respectively.

each modality: Mol-LLaMA (Kim et al., 2025) for molecule modality, Prot2Text-V2 (Fei et al., 2025) for protein modality, and Cell-o1 (Fang et al., 2025b) for single cell modality, whose base LLMs are LLaMA-3.1-8B-Instruct (Grattafiori et al., 2024). The merging methods are applied across all modality-specific models, resulting in a unified MLLM. Since each downstream task requires distinct domain knowledge, we provide task-specific few-shot in-context examples to induce the appropriate task understanding. For a fair comparison, we use the same instruction template and in-context examples for all compared methods. For more details for the implementation details, please refer to Appendix A.3 and A.4.

Baselines We compare ES-Merging with the base LLM, MLLMs specialized to a single modality, and merging methods. As modality-specialized baselines, we consider Mol-LLaMA, Prot2Text-V2, and Cell-o1, each specialized for molecule, protein, and single-cell modalities, respectively. We also compare ES-Merging with representative merging methods, including Average Merging, TIES-Merging (Yadav et al., 2023), EMR-Merging (Huang et al., 2024), layer-wise AdaMerging (Yang et al., 2023), PCB-Merging (Du et al., 2024), Consensus Merging (Wang et al., 2024b), LS-Merge (Soro et al., 2026), and task-specific fine-tuned model after the average merging, denoted as Avg. Merging + FT. For the base LLMs and the specialized MLLMs, unsupported modalities are

represented as textual inputs. Baseline details are provided in Appendix A.2.

5.2 Instance-varying Interaction Prediction

We first evaluate on instance-varying cross-modal interaction tasks, where the target counterpart changes across instances and the model should generalize across diverse cross-modal pairs.

Datasets We consider two instance-varying cross-modal interaction settings: molecule-protein interaction and molecule-cell interaction. For molecule-protein interaction, the task is to predict whether a given molecule interacts with a given protein, including BindingDB, BioSNAP, and Human (Koh et al., 2023). For molecule-cell interaction, the task is to predict the effect of a molecule on a given cell, including DrugComb (Zagidullin et al., 2019) and GDSC2 (Chawla et al., 2022). In both settings, the molecule, protein, and cell counterpart changes for each instance, requiring the model to generalize across diverse cross-modal combinations rather than relying on a fixed target identity. We provide the detailed explanation of datasets in Appendix A.1.

Results As shown in Table 1, ES-Merging consistently outperforms the merging baselines, suggesting that ES-Merging more effectively integrates complementary cross-modal knowledge from modality-specialized MLLMs and thus leading to stronger generalization when the interaction counterpart varies across instances. Notably, ES-

	CYP Inhibition												CYP Substrate							
	CYP1A2		CYP2C19		CYP2C9		CYP2D6		CYP3A4		Avg.		CYP2C9		CYP2D6		CYP3A4		Avg.	
	Acc.	F1	Acc.	F1	Acc.	F1	Acc.	F1	Acc.	F1	Acc.	F1	Acc.	F1	Acc.	F1	Acc.	F1	Acc.	F1
<i>Base LLM and Specialized MLLMs</i>																				
LLaMA-3.1-8B-Instruct	55.3	58.0	50.6	55.4	47.4	53.7	56.4	51.7	43.1	52.8	50.6	54.3	47.8	<u>50.7</u>	30.1	33.1	48.5	50.6	42.1	44.8
Mol-LLaMA	68.5	67.1	65.7	64.3	63.3	63.3	64.7	59.2	64.3	64.0	65.3	63.6	62.7	49.7	61.7	57.4	55.2	54.4	59.9	<u>53.8</u>
Prot2Text-V2	59.4	55.8	56.8	52.5	<u>67.4</u>	60.1	<u>76.3</u>	55.9	59.6	50.3	63.9	54.9	54.5	48.6	53.4	52.0	56.0	54.2	54.6	51.6
Cell-o1	53.5	58.3	44.9	51.9	43.1	52.8	46.9	46.3	43.6	51.6	46.4	52.2	36.6	41.7	36.1	39.9	48.5	55.0	40.4	45.6
<i>Merging Methods</i>																				
Avg. Merging	61.2	60.5	54.1	53.5	52.7	53.8	53.8	49.6	54.6	55.1	55.2	54.5	40.3	39.6	42.4	41.3	49.3	45.8	44.0	42.2
TIES-Merging	<u>71.8</u>	<u>71.8</u>	<u>67.8</u>	<u>67.9</u>	66.5	65.0	76.1	<u>64.0</u>	65.3	66.3	<u>69.5</u>	<u>67.0</u>	56.0	46.8	55.6	53.2	54.5	53.7	55.4	51.2
EMR-Merging	70.4	70.5	64.8	65.4	66.8	<u>66.3</u>	74.2	61.8	66.1	66.0	68.5	66.0	60.5	50.6	55.6	52.9	51.5	49.4	55.9	51.0
AdaMerging	52.5	55.3	53.1	54.2	44.8	46.0	45.6	45.7	50.4	54.3	49.3	51.1	33.6	33.6	43.6	45.7	49.3	47.4	42.2	42.2
PCB-Merging	69.2	69.4	63.6	64.6	65.0	63.8	72.4	61.0	63.8	65.2	66.8	64.8	55.2	44.9	57.1	53.9	<u>56.7</u>	55.7	56.4	51.5
Consensus Merging	68.5	68.8	63.6	64.1	65.7	64.0	73.5	60.8	63.8	64.7	67.0	64.5	54.5	46.5	55.6	52.9	<u>56.7</u>	<u>57.7</u>	55.6	52.4
LS-Merge	59.1	58.0	56.4	56.0	56.2	54.5	61.0	51.3	55.5	53.5	57.6	54.7	51.3	45.7	44.1	41.9	48.7	46.3	48.0	44.6
Avg. Merging + FT	68.3	67.7	67.0	66.5	62.2	62.1	67.6	60.9	<u>67.6</u>	<u>67.6</u>	66.5	65.0	65.7	50.6	59.4	53.0	55.2	54.6	<u>60.1</u>	52.7
ES-Merging (Ours)	77.4	77.4	70.6	70.5	72.5	70.4	80.7	69.5	71.3	70.8	74.5	71.7	<u>64.2</u>	53.6	<u>60.9</u>	<u>57.2</u>	60.5	59.6	61.9	56.8

Table 2: Performance comparison of ES-Merging on the target-fixed functionality prediction tasks. We report accuracy and macro-F1 across each subset. **Bold** indicates the best and underline indicates the second best.

Merging outperforms the task-specific finetuned model (Avg. Merging + FT) on the molecule-protein interaction tasks and shows comparable performance on the molecule-cell interaction tasks, indicating that ES-merging can enhance the cross-modal reasoning without further downstream fine-tuning. This superior performance of ES-Merging comes from preserving the reasoning capabilities of specialized MLLMs as shown in Table 5 and 6 in Appendix. In contrast, task-specific fine-tuning tends to diminish these reasoning capabilities and can even degrade performance, particularly on the molecule-protein interaction tasks. On the other hand, existing merging baselines such as EMR-Merging often exhibit substantial instability across datasets, showing a degraded performance on Drug-Comb. This implies that simple parameter space heuristics are insufficient for reliably combining heterogeneous multimodal experts, supporting that ES-Merging provides a more robust integration of modality-specific knowledge.

5.3 Target-fixed Functionality Prediction

We further evaluate on target-fixed cross-modal functionality prediction tasks, where each subtask is associated with a fixed target and requires target-specific biological functionality knowledge beyond simple interaction matching in Section 5.2.

Datasets To this end, we evaluate on CYP enzyme prediction. Unlike the instance-varying setting above, each subtask is defined with respect to a fixed enzyme target and the tasks are predicting the biological functionality of the given molecule to the fixed target: inhibitory effects

or substrate specificity. Specifically, we consider five CYP inhibition subtasks to CYP1A2, CYP2C19, CYP2C9, CYP2D6, and CYP3A4 enzymes (Weiser et al., 2023), and three CYP substrate subtasks for CYP2C9, CYP2D6, and CYP3A4 enzymes (Holmer et al., 2021), from the TDC dataset (Huang et al., 2021). These benchmarks therefore evaluate whether the merged model can capture not only detailed molecular structural variation under a shared target, but also biologically meaningful interaction types.

Results As shown in Table 2, ES-Merging achieves the best average performance, suggesting that it more effectively preserves and integrates expert knowledge required for target-specific functionality prediction. In contrast, on the CYP substrate tasks, most merging baselines underperform Mol-LLaMA, likely because these tasks rely heavily on molecular structural understanding under a fixed-target setting. Notably, ES-Merging achieves performance that is comparable to or better than Mol-LLaMA, suggesting that embedding-signal-based merging can not only integrate modality-specific expertise more effectively but also enhance cross-modal understanding.

5.4 Ablation Study

We further conduct an ablation study to see the effectiveness of each coefficient type. As shown in Table 3, using only one of coefficient types still outperforms other merging baselines, indicating that the embedding space signals provide salient and robust information for cross-modal merging, compared to the merging methods based on the

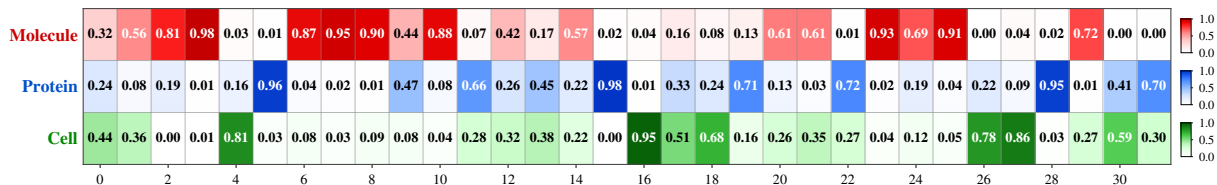


Figure 5: Computed layer-wise merging coefficient visualization of each specialized MLLM derived by Eq. 2. The l -th column corresponds to the merging coefficient of the l -th layer, $\alpha_{m_j}^l$.

Coefficient Type	Instance-varying		Target-fixed	
	Mol-Prot	Mol-Cell	CYP Inhib.	CYP Subs.
Layer-wise	63.6	85.2	73.9	57.1
Element-wise	64.9	86.7	72.7	60.5
Layer×Element	65.7	87.4	74.5	61.9

Table 3: Ablation studies on merging coefficient types. We report average accuracy on each task group.

Method	Total FLOPs ↓
Avg. Merging + FT	891,117
AdaMerging	493,694
ES-Merging (Ours)	149,807

Table 4: Total Floating Point Operations (FLOPs) as a measure of computational cost for determining the merging coefficients and LoRA module parameters

parameter space signals. On the other hand, combining two different coefficients shows the best performance, enabling to capture different granularities of MLLMs’ specialization.

5.5 Merging Coefficient Analysis

We visualize the layer-wise merging coefficients in Fig. 5 and the element-wise merging coefficients in Fig. 9 of Appendix. The coefficients are distinctly distributed across different MLLMs, showing that modality-specific knowledge is not incorporated uniformly throughout the model. Additionally, we observe that even when the layer-wise coefficient is high (e.g., the third layer of the molecule LLM), the element-wise merging coefficients within that layer vary substantially, as shown in Fig. 6. This result indicates that modality specialization emerges at multiple levels of granularity: only a few parameter elements within important layers are primarily salient for modality specialization. Therefore, combining layer-wise global coefficients with element-wise local coefficients leads to the complementary merging of different granularities, achieving an accurate and robust merging of different modalities.

5.6 Computational Cost Comparison

We compare the computation cost with the baselines requiring the computation of gradients and parameter updates. As shown in Table 4, the com-

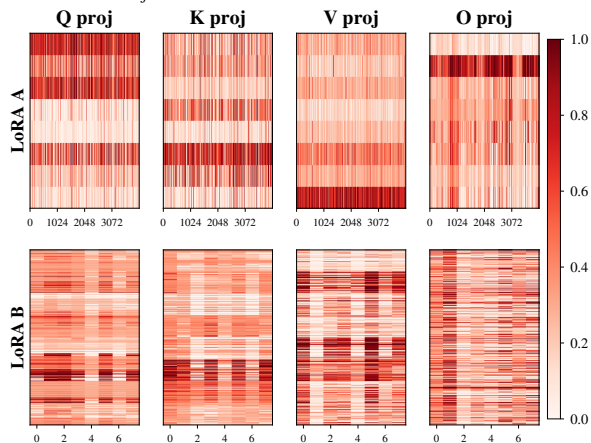


Figure 6: Computed element-wise merging coefficient visualization of each module in the third layer of molecule LLM derived by Eq. 3.

putational cost of ES-Merging is $3.4\times$ and $6.1\times$ lower than AdaMerging and Task-specific Finetuning respectively, since ES-Merging requires the gradient computation only one time, while other baselines iteratively compute gradients and update parameters. While ES-Merging requires less computational cost, it outperforms the Task-specific Finetuning and AdaMerging, indicating the efficiency and effectiveness of ES-Merging.

6 Conclusion

We present ES-Merging, a novel MLLM merging framework that shifts model merging from relying on parameter space signals to leveraging embedding space signals. Our key insight is that input-aware representations encode rich modality-specific specialization, providing a more faithful basis for integrating modality-specialized MLLMs. Based on this observation, we introduce two complementary types of merging coefficients at different granularities: layer-wise global coefficients for capturing coarse-grained specialization and element-wise local coefficients for capturing fine-grained importance. Experiments on interactive effect prediction tasks demonstrate that ES-Merging consistently improves multimodal merging performance across diverse biological tasks, highlighting embedding space signals as a principled foundation for MLLM merging.

References

- Hadi Abdine, Michail Chatzianastasis, Costas Bouyioukos, and Michalis Vazirgiannis. 2024. Prot2text: Multimodal protein’s function generation with gnn and transformers. In *Proceedings of the AAAI conference on artificial intelligence*, volume 38, pages 10757–10765.
- Nicolas Bonneel, Julien Rabin, Gabriel Peyré, and Hanspeter Pfister. 2015. Sliced and radon wasserstein barycenters of measures. *Journal of Mathematical Imaging and Vision*, 51(1):22–45.
- He Cao, Zijing Liu, Xingyu Lu, Yuan Yao, and Yu Li. 2023. Instructmol: Multi-modal integration for building a versatile and reliable molecular assistant in drug discovery. *arXiv:2311.16208*.
- Saurabh Chawla, Anja Rockstroh, Melanie Lehman, and 1 others. 2022. [Gene expression based inference of cancer drug sensitivity](#). *Nature Communications*, 13(1):5680.
- Chi-Jane Chen, Yuhang Chen, Sukwon Yun, Natalie Stanley, and Tianlong Chen. 2025. Spatial coordinates as a cell language: A multi-sentence framework for imaging mass cytometry analysis. In *Findings of the Association for Computational Linguistics: ACL 2025*, pages 13241–13252.
- Seyone Chithrananda, Gabriel Grand, and Bharath Ramsundar. 2020. Chemberta: large-scale self-supervised pretraining for molecular property prediction. *arXiv:2010.09885*.
- Gheorghe Comanici, Eric Bieber, Mike Schaekermann, Ice Pasupat, Noveen Sachdeva, Inderjit Dhillon, Marcel Blistein, Ori Ram, Dan Zhang, Evan Rosen, and 1 others. 2025. Gemini 2.5: Pushing the frontier with advanced reasoning, multimodality, long context, and next generation agentic capabilities. *arXiv preprint arXiv:2507.06261*.
- Sajib Acharjee Dip, Adrika Zafor, Bikash Kumar Paul, Uddip Acharjee Shuvo, Muhit Islam Emon, Xuan Wang, and Liqing Zhang. 2025. Llm4cell: A survey of large language and agentic models for single-cell biology. *arXiv preprint arXiv:2510.07793*.
- Guodong Du, Junlin Lee, Jing Li, Runhua Jiang, Yifei Guo, Shuyang Yu, Hanting Liu, Sim K Goh, Ho-Kin Tang, Daojing He, and 1 others. 2024. Parameter competition balancing for model merging. *Advances in Neural Information Processing Systems*, 37:84746–84776.
- Carl Edwards, Tuan Lai, Kevin Ros, Garrett Honke, Kyunghyun Cho, and Heng Ji. 2022. Translation between molecules and natural language. In *Proceedings of the 2022 Conference on Empirical Methods in Natural Language Processing*, pages 375–413.
- Yin Fang, Xinle Deng, Kangwei Liu, Ningyu Zhang, Jingyang Qian, Penghui Yang, Xiaohui Fan, and Huajun Chen. 2025a. A multi-modal ai copilot for single-cell analysis with instruction following. *arXiv preprint arXiv:2501.08187*.
- Yin Fang, Qiao Jin, Guangzhi Xiong, Bowen Jin, Xi-anrui Zhong, Siru Ouyang, Aidong Zhang, Jiawei Han, and Zhiyong Lu. 2025b. Cell-o1: Training llms to solve single-cell reasoning puzzles with reinforcement learning. *arXiv preprint arXiv:2506.02911*.
- Yin Fang, Xiaozhuan Liang, Ningyu Zhang, Kangwei Liu, Rui Huang, Zhuo Chen, Xiaohui Fan, and Huajun Chen. 2023. Mol-instructions: A large-scale biomolecular instruction dataset for large language models. *arXiv preprint arXiv:2306.08018*.
- Xiao Fei, Michail Chatzianastasis, Sarah Almeida Carneiro, Hadi Abdine, Lawrence P Petalidis, and Michalis Vazirgiannis. 2025. Prot2text-v2: Protein function prediction with multimodal contrastive alignment. *Advances in Neural Information Processing Systems*.
- Aaron Grattafiori, Abhimanyu Dubey, Abhinav Jauhri, Abhinav Pandey, Abhishek Kadian, Ahmad Al-Dahle, Aiesha Letman, Akhil Mathur, Alan Schelten, Alex Vaughan, and 1 others. 2024. The llama 3 herd of models. *arXiv preprint arXiv:2407.21783*.
- Han Guo, Mingjia Huo, Ruiyi Zhang, and Pengtao Xie. 2023. Proteinchat: Towards achieving chatgpt-like functionalities on protein 3d structures. *Authorea Preprints*.
- Shuhan Guo, Yatao Bian, Ruibing Wang, Nan Yin, Zhen Wang, and Quanming Yao. 2024. Unimot: Unified molecule-text language model with discrete token representation. *arXiv preprint arXiv:2408.00863*.
- Malte Holmer, Christina de Bruyn Kops, Conrad Stork, and Johannes Kirchmair. 2021. [Cypstrate: A set of machine learning models for the accurate classification of cytochrome p450 enzyme substrates and non-substrates](#). *Molecules*, 26(15):4678.
- Edward J Hu, Yelong Shen, Phillip Wallis, Zeyuan Allen-Zhu, Yuanzhi Li, Shean Wang, Liang Wang, Weizhu Chen, and 1 others. 2022. Lora: Low-rank adaptation of large language models. *ICLR*, 1(2):3.
- Chenyu Huang, Peng Ye, Tao Chen, Tong He, Xianguyu Yue, and Wanli Ouyang. 2024. Emr-merging: Tuning-free high-performance model merging. *Advances in Neural Information Processing Systems*, 37:122741–122769.
- Kexin Huang, Tianfan Fu, Wenhao Gao, Yue Zhao, Yusuf Roohani, Jure Leskovec, Connor W Coley, Cao Xiao, Jimeng Sun, and Marinka Zitnik. 2021. Therapeutics data commons: Machine learning datasets and tasks for drug discovery and development. *arXiv preprint arXiv:2102.09548*.
- Gabriel Ilharco, Marco Tulio Ribeiro, Mitchell Wortsman, Suchin Gururangan, Ludwig Schmidt, Hannaneh Hajishirzi, and Ali Farhadi. 2022. Editing models with task arithmetic. *arXiv preprint arXiv:2212.04089*.

- Oussama Kharouiche, Aris Markogiannakis, Xiao Fei, Michail Chatzianastasis, and Michalis Vazirgiannis. 2025. Cell2text: Multimodal llm for generating single-cell descriptions from rna-seq data. *arXiv preprint arXiv:2509.24840*.
- Dongki Kim, Wonbin Lee, and Sung Ju Hwang. 2025. Mol-llama: Towards general understanding of molecules in large molecular language model. *Advances in Neural Information Processing Systems*.
- Huan Yee Koh, Anh T.N. Nguyen, Shirui Pan, Lauren T. May, and Geoffrey I. Webb. 2023. **Psichic: physicochemical graph neural network for learning protein-ligand interaction fingerprints from sequence data.** *bioRxiv*.
- Mario Krenn, Florian Häse, AkshatKumar Nigam, Pascal Friederich, and Alan Aspuru-Guzik. 2020. Self-referencing embedded strings (selfies): A 100% robust molecular string representation. *Machine Learning: Science and Technology*, 1(4):045024.
- Longyi Li, Liyan Dong, Hao Zhang, Dong Xu, and Yongli Li. 2025. spallm: enhancing spatial domain analysis in multi-omics data through large language model integration. *Briefings in Bioinformatics*, 26(4):bbaf304.
- Sihang Li, Zhiyuan Liu, Yanchen Luo, Xiang Wang, Xiangnan He, Kenji Kawaguchi, Tat-Seng Chua, and Qi Tian. 2024. Towards 3d molecule-text interpretation in language models. *arXiv preprint arXiv:2401.13923*.
- Zeming Lin, Halil Akin, Roshan Rao, Brian Hie, Zhongkai Zhu, Wenting Lu, Allan dos Santos Costa, Maryam Fazel-Zarandi, Tom Sercu, Sal Candido, and 1 others. 2022. Language models of protein sequences at the scale of evolution enable accurate structure prediction. *BioRxiv*, 2022:500902.
- Zhiyuan Liu, Sihang Li, Yanchen Luo, Hao Fei, Yixin Cao, Kenji Kawaguchi, Xiang Wang, and Tat-Seng Chua. 2023. MolCA: Molecular graph-language modeling with cross-modal projector and uni-modal adapter. In *Proceedings of the 2023 Conference on Empirical Methods in Natural Language Processing*.
- Zhenyi Lu, Chenghao Fan, Wei Wei, Xiaoye Qu, Danyang Chen, and Yu Cheng. 2024. Twin-merging: Dynamic integration of modular expertise in model merging. *Advances in Neural Information Processing Systems*, 37:78905–78935.
- OpenAI. 2024a. Gpt-4 technical report. *arXiv:2303.08774*.
- OpenAI. 2024b. Gpt-4o system card. *arXiv:2410.21276*.
- Jinyoung Park, Minseong Bae, Dohwan Ko, and Hyunwoo J Kim. 2024. Llamol: Large language model-based molecular graph assistant. *Advances in Neural Information Processing Systems*, 37:131972–132000.
- Qizhi Pei, Wei Zhang, Jinhua Zhu, Kehan Wu, Kaiyuan Gao, Lijun Wu, Yingce Xia, and Rui Yan. 2023. Biot5: Enriching cross-modal integration in biology with chemical knowledge and natural language associations. In *Proceedings of the 2023 Conference on Empirical Methods in Natural Language Processing*, pages 1102–1123.
- Syed Asad Rizvi, Daniel Levine, Aakash Patel, Shiyang Zhang, Eric Wang, Curtis Jamison Perry, Nicole Mayerli Constante, Sizhuang He, David Zhang, Cerise Tang, and 1 others. 2025. Scaling large language models for next-generation single-cell analysis. *BioRxiv*, pages 2025–04.
- David Rogers and Mathew Hahn. 2010. Extended-connectivity fingerprints. *Journal of chemical information and modeling*, 50(5):742–754.
- Bedionita Soro, Aoxuan Silvia Zhang, Bruno Andreis, Jaehyeong Jo, Song Chong, and Sung Ju Hwang. 2026. Ls-merge: Merging language models in latent space. In *The Fourteenth International Conference on Learning Representations*.
- Hugo Touvron and 1 others. 2023. Llama 2: Open foundation and fine-tuned chat models. *arXiv:2307.09288*.
- Chao Wang, Hehe Fan, Ruijie Quan, and Yi Yang. 2024a. Protchatgpt: Towards understanding proteins with large language models. *arXiv preprint arXiv:2402.09649*.
- Ke Wang, Nikolaos Dimitriadis, Guillermo Ortiz-Jimenez, François Fleuret, and Pascal Frossard. 2024b. Localizing task information for improved model merging and compression. *arXiv preprint arXiv:2405.07813*.
- Zhicong Wang, Zicheng Ma, Ziqiang Cao, Changlong Zhou, Jun Zhang, and Yi Qin Gao. 2025a. Prot2chat: protein large language model with early fusion of text, sequence, and structure. *Bioinformatics*, 41(8):btaf396.
- Ziqing Wang, Kexin Zhang, Zihan Zhao, Yibo Wen, Abhishek Pandey, Han Liu, and Kaize Ding. 2025b. A survey of large language models for text-guided molecular discovery: from molecule generation to optimization. *arXiv preprint arXiv:2505.16094*.
- David Weininger. 1988. Smiles, a chemical language and information system. 1. introduction to methodology and encoding rules. *Journal of chemical information and computer sciences*, 28(1):31–36.
- Benjamin Weiser, Jérôme Genzling, Mihai Burai-Patrascu, Ophélie Rostaing, and Nicolas Moitessier. 2023. **Machine learning-augmented docking. 1. cyp inhibition prediction.** *Digital Discovery*, 2:1841–1849.
- Peter Willett, John M Barnard, and Geoffrey M Downs. 1998. Chemical similarity searching. *Journal of chemical information and computer sciences*, 38(6):983–996.

- Yijia Xiao, Edward Sun, Yiqiao Jin, Qifan Wang, and Wei Wang. 2024. Proteingpt: Multimodal llm for protein property prediction and structure understanding. *arXiv preprint arXiv:2408.11363*.
- Yijia Xiao, Wanxia Zhao, Junkai Zhang, Yiqiao Jin, Han Zhang, Zhicheng Ren, Renliang Sun, Haixin Wang, Guancheng Wan, Pan Lu, and 1 others. 2025. Protein large language models: A comprehensive survey. *arXiv preprint arXiv:2502.17504*.
- Minghao Xu, Xinyu Yuan, Santiago Miret, and Jian Tang. 2023. Protst: Multi-modality learning of protein sequences and biomedical texts. In *International conference on machine learning*, pages 38749–38767. PMLR.
- Prateek Yadav, Derek Tam, Leshem Choshen, Colin A Raffel, and Mohit Bansal. 2023. Ties-merging: Resolving interference when merging models. *Advances in neural information processing systems*, 36:7093–7115.
- Enneng Yang, Zhenyi Wang, Li Shen, Shiwei Liu, Guibing Guo, Xingwei Wang, and Dacheng Tao. 2023. Adamerging: Adaptive model merging for multi-task learning. *arXiv preprint arXiv:2310.02575*.
- Botao Yu, Frazier N. Baker, Ziqi Chen, Xia Ning, and Huan Sun. 2024. Llasmol: Advancing large language models for chemistry with a large-scale, comprehensive, high-quality instruction tuning dataset. *arXiv preprint arXiv:2402.09391*.
- Bulat Zagidullin, Jehad Aldahdooh, Shuyu Zheng, Wenyu Wang, Yinyin Wang, Joseph Saad, Alina Maljutina, Mohieddin Jafari, Ziaurrehman Tanoli, Alberto Pessia, and Jing Tang. 2019. **Drugcomb: an integrative cancer drug combination data portal**. *Nucleic Acids Research*, 47(W1):W43–W51.

Organization Appendix is organized as follows: In Section A, we provide detailed experimental settings, including datasets, baseline, implementation, and prompt setting details. In Section B, we qualitatively analyze generated responses. In Section C, we provide additional analysis of our merging method. In Section D, we discuss the limitations of our work.

A Experiment Settings

A.1 Datasets Detail

- **BindingDB** is a drug-target interaction dataset derived from experimentally measured small molecule-protein binding data, typically filtered to human proteins, and used as a binary classification benchmark with 11,054 samples for predicting whether a drug-target pair interacts.
- **BioSNAP** is a drug-target interaction dataset derived from known associations between US-marketed drugs and their human protein targets, and is used as a binary classification benchmark with 6,058 samples for predicting whether a drug-target pair interacts.
- **Human** is a drug-target interaction dataset consisting of drug-human protein pairs with highly credible negative samples and used as a binary classification benchmark with 1,375 samples to predict whether a drug-target pair interacts.
- **DrugComb** is a drug combination-cell line interaction dataset derived from standardized and harmonized drug combination screening studies across various cancer cell lines, and is used as a binary classification benchmark with 3,631 samples for predicting whether a combination of two drugs produces a synergistic or antagonistic anti-cancer effect in a given cancer cell line.
- **GDSC2** is a drug-cell line interaction dataset derived from the Genomics of Drug Sensitivity in Cancer project, which screens over 1,000 genetically characterized human cancer cell lines with a wide range of anti-cancer therapeutics using a newer cell screening platform introduced in 2015, and is used as a binary classification benchmark with 843 samples for predicting whether a given cancer cell line is sensitive or resistant to a specific drug.
- **CYP1A2, CYP2C19, CYP2C9, CYP2D6, and CYP3A4 Inhibition** are binary classification benchmarks for predicting whether a given drug

inhibits a specific cytochrome P450 enzyme isoform involved in drug metabolism, consisting of 2,516, 2,533, 2,418, 2,626, and 2,466 samples, respectively.

- **CYP2C9, CYP2D6, and CYP3A4 Substrate** are three binary classification benchmarks to predict whether a given drug is a substrate of a specific cytochrome P450 enzyme isoform involved in drug metabolism with 134, 133, and 134 samples, respectively.

A.2 Baseline Detail

We compare our method against three modality-specialized base models, one task-specific fine-tuned model, six existing model merging baselines, and three ablation variants of our proposed method.

- **Mol-LLaMA** (Kim et al., 2025) is a large molecular language model trained via multi-modal instruction tuning that integrates complementary 2D and 3D molecular encoders through a blending module, with a Q-Former projector and a LLaMA backbone fine-tuned with LoRA, providing general molecular understanding with explainability and reasoning capabilities across diverse molecular tasks.
- **Prot2Text-V2** (Fei et al., 2025) is a multi-modal sequence-to-text model that combines an ESM2-3B (Lin et al., 2022) protein sequence encoder with a LLaMA-3.1-8B-Instruct decoder via a nonlinear modality projector, using hybrid sequence-level contrastive alignment learning and instruction-based LoRA fine-tuning to generate rich functional descriptions of proteins directly from amino acid sequences.
- **Cell-o1** (Fang et al., 2025b) is a cell line-specialized model fine-tuned on transcriptomic omics data, capable of handling cell line-related drug response tasks but limited to single-modality inference without understanding molecule or protein.
- **Average Merging** directly averages the parameter elements of all specialist MLLMs parameters without any additional computation.
- **Average Merging + Task-Specific Finetune** constructs a base model by averaging the LoRA weights of all three specialist models, and subsequently fine-tunes the LoRA parameters independently on each evaluation task by sampling 2,000 examples from the training dataset for 10 epochs with a batch size of 16.

- **TIES-Merging** (Yadav et al., 2023) resolves interference among task vectors through three steps, trim, elect sign, and disjoint merge, which prune low-magnitude parameters, resolve sign conflicts by selecting the dominant direction, and merge only the parameter-aligned subset.
- **AdaMerging** (Yang et al., 2023) learns merging coefficients for task vectors in a test-time adaptation manner, using the minimization of model output entropy on unlabeled test samples as a surrogate objective without relying on original training data. In our experiments, we adopt the layer-wise AdaMerging variant which independently learns a merging coefficient for each layer of every task vector, showing better performance compared to the task-wise AdaMerging.
- **EMR-Merging** (Huang et al., 2024) is a tuning-free method that first elects a unified task vector by selecting the maximum absolute value of each parameter along the dominant sign direction, and then generates lightweight task-specific masks and rescalers to align the direction and magnitude of the unified model with each original specialist model at inference time.
- **PCB-Merging** (Du et al., 2024) is a training-free method that constructs a parameter competition balancing matrix through intra-balancing, which measures parameter significance within individual tasks, and inter-balancing, which assesses parameter similarity across tasks, then drops low-scoring parameters and rescales the remaining ones to form the final merged model.
- **Consensus-Merging** (Wang et al., 2024b) identifies and removes two classes of detrimental parameters, selfish weights that are critical exclusively to a single task and catastrophic weights that are irrelevant to all tasks and retains only the consensus parameters that contribute positively to multi-task fusion.
- **LS-Merge** (Soro et al., 2026) encodes model weights into a latent space via a transformer-based VAE, performs merging through linear interpolation in that space, and decodes back to parameters.
- **Layer-wise ES-Merging (Ours)** applies only the layer-wise global coefficient $\alpha_{m_j}^l$, derived from SWD-based embedding distribution shifts between the base and specialized models, as the merging coefficient.
- **Element-wise ES-Merging (Ours)** applies only the element-wise local coefficient $\beta_{m_j}^{l,n}$, derived from gradient-based parameter sensitivity scores with respect to fine-grained embedding distances, as the merging coefficient.
- **ES-Merging (Ours)** integrates both the global layer coefficient $\alpha_{m_i}^l$ and the local element coefficient $\beta_{m_i}^{l,n}$ into a unified merging coefficient $\lambda_{m_i}^{l,n}$ by multiplication and renormalization of elements in modalities.

A.3 Implementation Details

LoRA Configuration All specialized models used for merging share a unified LoRA (Hu et al., 2022) configuration with rank $r = 8$, and scaling factor $\alpha = 32$, applied to all self-attention projection matrices ($\mathbf{W}_Q, \mathbf{W}_K, \mathbf{W}_V, \mathbf{W}_O$) and MLP projection layers (gate, up, and down projections) of every transformer block.

Details of ES-Merging To construct the probe inputs, we randomly sample the 110 samples for each modality from a collection of test sets, constructing 330 samples in total. For the layer-wise merging coefficient computation, we leverage SWD with slice projection $\text{dim}=1,024$ and distance order $p=2.0$, then normalized via softmax with temperature $\tau=0.5$. For the element-wise merging coefficient computation, the temperature τ of the softmax is predefined as 0.5.

Existing Merging Methods For all baseline methods, we follow the experimental settings reported in their respective original papers and official implementations. For LS-Merge (Soro et al., 2026), we train VAE with sequence length 16,384, batch size 512, learning rate 3×10^{-4} with 500 step warmup and cosine decay, and KL weight 10^{-4} with adaptive adjustment toward a target KL of 50, for 1,000 epochs. At merge time, model parameters are split into chunks of size 16,384, encoded into the latent space via the VAE encoder, merged via uniform-weighted Euclidean mean of the posterior means μ , and decoded back to parameter space.

A.4 Prompt Setting for Evaluation

To impart the task-specific knowledge, we provide 5-shot examples from the training set with the prompt templates in

Table 9 and Table 10. The retrieval strategy is designed per task as follows:

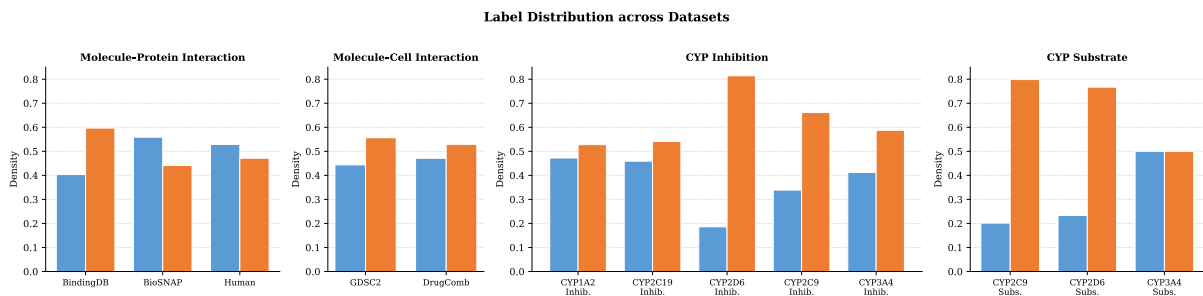


Figure 7: Label distribution across datasets. Each panel shows positive and negative sample counts for Molecule-Protein Interaction, CYP Inhibition, CYP Substrate, and Molecule-Cell Interaction tasks.

- Molecule-Protein Interaction:** Training samples whose target protein sequence exactly matches the query are first collected. If more than five exact matches exist, the top-5 are selected by Tanimoto similarity (Willett et al., 1998) of Morgan fingerprints (Rogers and Hahn, 2010) between their molecules and the query molecule. If fewer than five are found, the remaining slots are filled with samples from proteins with the highest cosine similarity of protein embeddings from ESM2 to the query protein. Among candidates from the same similar protein, the one with the highest Tanimoto similarity to the query molecule is preferred.
- Drug-Cell Interaction:** Training samples whose cell line shares an exact match on the top-50 expressed gene set are priorly collected. If fewer than five are found, additional samples are drawn from cell lines with the highest Jaccard similarity on gene sets. When multiple candidates exist from the same cell line, the one with the highest Tanimoto similarity to the query molecule is selected. For DrugComb, molecule similarity is computed as the average Tanimoto similarity across both drugs.
- CYP Inhibition/Substrate:** Since all samples share the same CYP enzyme target, protein-level filtering is unnecessary. The top-5 examples are selected solely by Tanimoto similarity between the training molecules and the query molecule.

A.5 Evaluation Metric

As shown in Figure 7, while some datasets exhibit a relatively balanced distribution between positive and negative samples, others such as BindingDB and CYP2D6 Inhibition display a pronounced class imbalance. In particular, the CYP Substrate task contains only approximately 130 samples per dataset, posing a critical challenge of absolute data

scarcity. In such imbalanced and low resource settings, relying solely on accuracy as an evaluation metric can be misleading, as a model that predominantly predicts the majority class may still achieve inflated scores without genuinely capturing minority-class patterns. Therefore, we leverage the macro-F1 that addresses this limitation by computing the F1 score for each class independently and averaging them with equal weight regardless of class frequency, thereby providing a fair assessment of predictive performance across all classes.

B Qualitative Analysis

In this section, we qualitatively compare the generated responses of each task-specific fine-tuned model with those of ES-Merging, as shown in Table 5 and Table 6.

B.1 Molecule-Protein Interaction Prediction

Table 5 presents a generated response on the molecule-protein interaction prediction task from the Human dataset, where the molecule is thymine and the target protein is thymidine phosphorylase. Although both ES-Merging and the task-specific finetuning model correctly predict the label, the two responses differ substantially in quality. ES-Merging correctly identifies thymine as a pyrimidine base found in DNA and a heterocyclic aromatic compound, then progressively reasons through its biological context, such as base pairing with adenine and its role in DNA synthesis, to conclude that thymine is likely to interact with the protein as a substrate for enzymes involved in thymidine metabolism. This can be interpreted as evidence that the chemical structure-level knowledge acquired from the molecule expert model and the biological function-level knowledge acquired from the protein expert model are organically integrated within a single model through embedding

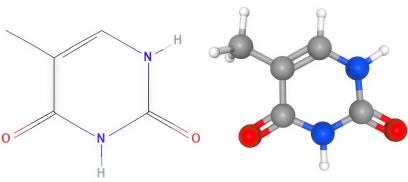
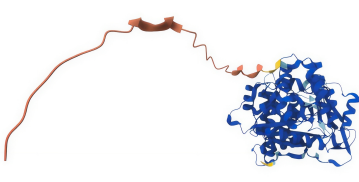
	
Input Molecule	Input Protein
Molecule Name: Thymine	
SMILES: <chem>CC1=CNC(=O)NC1=O</chem>	
Protein: Thymidine phosphorylase	
Protein Sequence: MAALMTPGTGAPPAPGDFSGEGSQGLPDPSPPEPKQLPELIRMKRDRGGRLSEADIRGFVAAVVN GSAQGAQIGAMLMAIRLRGMDLEETSVLQALAQSGQQLWPEAWRQQLVDKHSTGGVGDKVSLLVAPALAACGC KVPMSIGRGLGHTGGTLDKLESIPGFNVISPEQMQLLDQAGCCIVGQSEQLVPADGILYAARDVTATVDSLPLITAS ILSKKLVEGLSALVVDVKFGGAAVFPNQEQARELAKTLVGVGASLGLRVAAALTAMDKPLGRCVGHAVEVEALLC MDGAGPPDLRDLVTTLLGALLWLSGHAGTQAQGAARVAAALDDGSALGRFERMLAAQGVDPGLARALCSGSPAER RQLLPRAREQEELLAPADGTVELVRALPLALVLHELGAGRSRAGEPLRLGVGAELLVDVGQQLRRGTPWLRVHRDGP ALSGPQSRALQEALVLSRAPFAAPSPFAELVLPQQ	
User: Determine whether the given molecule interacts with the protein by following the example.	
Ground Truth: Interacts	
ES-Merging (Ours) The given molecule is thymine, a pyrimidine base found in DNA and RNA. It is a heterocyclic aromatic organic compound. The protein is not specified, but based on the examples, it is likely a DNA or RNA polymerase enzyme. Thymine is a nucleobase that pairs with adenine in DNA. It is also a substrate for thymidylate synthase, an enzyme that catalyzes the conversion of uracil to thymine in DNA synthesis. Given the information, it is likely that the molecule interacts with the protein, as thymine is a substrate for thymidylate synthase, an enzyme that catalyzes a critical step in DNA synthesis. Final answer: Interacts.	
Models with Avg. + Task-Specific Finetuning Final answer: Interacts	

Table 5: Case study on Molecule-Protein Interaction prediction.

space signal-based merging. In contrast, the task-specific finetuned model outputs only the label “Interacts” without any biological rationale. Because it was trained on instruction data containing labels only, its predictions are less interpretable, whereas ES-Merging integrates modality-expert knowledge to produce interpretable reasoning even for unseen cross-modal tasks.

B.2 Molecule-Cell Interaction Prediction

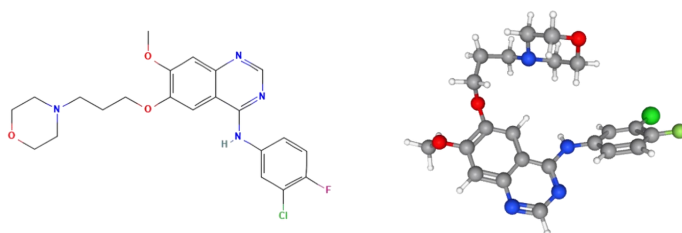
Table 6 presents a qualitative analysis of the Drug-Cell Interaction prediction task from the GDSC2 dataset, where the drug is Gefitinib, and the cell line is OVCA420.

ES-Merging first identifies the given molecule as a quinazoline derivative and correctly recognizes it as a potent inhibitor of the epidermal growth factor receptor (EGFR) tyrosine kinase. It also accurately identifies the given cell line as a cancer cell, then focuses on genes such as RPS6, EIF1,

and GNB2L1 in the ranked gene-expression list to interpret the cell as actively proliferating and potentially dependent on EGFR signaling. On the basis of this, ES-Merging correctly recognizes that the drug’s mechanism of action is effective against the given cell. This reasoning chain spanning from molecular substructure to drug class, target pathway, cell type identification, and cell-level interpretation demonstrates that the structural knowledge from the molecule expert model and the transcriptomic knowledge from the cell expert model are functionally integrated through ES-Merging, while the model with task-specific finetuning again outputs only the label “Sensitive” without any biological rationale.

C Further Analysis

In this section, we provide a detailed analysis of the merging coefficients used in ES-Merging, extended results of the ablation study in the main paper, and



Drug Name: Gefitinib

SMILES: COC1=C(C=C2C(=C1)N=CN=C2NC3=CC(=C(C=C3)F)C1)OCCCN4CCOCC4

Cell Line: OVCA420

Top 50 Genes: RPL35, FTL, MT-ND4, GAPDH, AKR1B10, UBC, RPS6, RPL24, EIF1, GNB2L1, SPP1, RPS11, AKR1C1, RPL19, GNG5, AKR1B10P1, ACTG1, MT-CO3, RPL5, FAU, RPS15A, TXN, RPL8, MIF, LDHB, KRT19, EIF4H, RPL11, ALDH1A1, MGST1, RPS12, CLIC1, SNRPD2, RPL30, H2AFX, NQO1, PRDX1, RPS5, RPLP1, H2AFZ, TUBB4B, FAUP1, NACA, RPL14, HIST1H2BK, MYL12B, SHFM1P1, HINT1P1, RPL27, HIST1H4C

User: Determine whether the given cell is sensitive or resistant to the given molecule based on the ranked gene-expression list.

Ground Truth: Sensitive

ES-Merging (Ours)

The given molecule is 4-(3-fluoro-4-methoxyphenyl)-7-methyl-6-oxo-1,4-dihydroquinazoline-3-carboximidamide, which is a quinazoline derivative. This type of molecule is known to be a potent inhibitor of the epidermal growth factor receptor (EGFR) tyrosine kinase. The cell line provided is a cancer cell, and the presence of genes such as RPS6, EIF1, and GNB2L1 in the list suggests that the cell is actively proliferating and may be dependent on EGFR signaling for growth and survival. Given the presence of these genes and the fact that the molecule is an EGFR inhibitor, it is likely that the cell is sensitive to the molecule.

Final answer: Sensitive

Models with Avg. + Task-Specific Finetuning

Final answer: Sensitive

Table 6: Case study on Molecule-Cell Interaction prediction.

an analysis of embedding visualizations.

C.1 Merging Coefficients

C.1.1 Layer-wise Merging Coefficients

Size	Human	GDSC2	CYP2C9 Inh.	CYP2C9 Sub.
32	60.7	90.6	68.2	53.7
256	62.0	93.1	68.9	48.5
1024	62.0	94.1	72.5	64.2

Table 7: Ablation studies on projection size of SWD for layer-wise ES-Merging across Molecule-Protein and Molecule-Cell Interaction tasks.

Projection Dimension Size of SWD When computing SWD for the layer-wise merging coefficients, we vary projection dimension sizes on representative datasets for each task, and derived merging coefficients accordingly. As shown in Table 7, performance consistently improves as the projection size increases, with 1024 dimensions achiev-

ing the best results. This is because a larger number of projections enables a more precise approximation of the distributional differences in high-dimensional space, leading to more accurate computation of the layer-wise merging coefficients. Based on this finding, we set the SWD projection size to 1024 in our main experiments.

C.1.2 Element-wise Merging Coefficients

The coefficient patterns differ across q/k/v/o_proj modules even within the same layer. As shown in Figure 9, the q/k/v projection modules and the o projection module emphasize different elements even at Layer 0. Within the same module, the coefficient distributions between LoRA A and LoRA B exhibit distinct patterns. In particular, at Layer 0 of the q projection module, LoRA A shows relatively balanced coefficients across all modalities, whereas LoRA B contains regions where molecule and protein are more prominent. On the other hand,

Coefficient Type	Molecule-Protein Interaction				Molecule-Cell Interaction			CYP Inhibition					CYP Substrate				
	BindingDB	BioSNAP	Human	Avg.	DrugComb	GDSC2	Avg.	CYP1A2	CYP2C19	CYP2C9	CYP2D6	CYP3A4	Avg.	CYP2C9	CYP2D6	CYP3A4	Avg.
Layer-wise	65.5	<u>68.2</u>	57.0	63.6	<u>80.1</u>	<u>90.2</u>	<u>85.2</u>	<u>76.3</u>	71.4	<u>72.3</u>	<u>79.2</u>	<u>70.2</u>	<u>73.9</u>	61.2	54.9	55.2	57.1
Element-wise	66.5	66.6	<u>61.4</u>	<u>64.9</u>	79.3	94.1	86.7	76.0	69.1	70.7	77.6	69.8	<u>72.7</u>	65.7	<u>57.6</u>	<u>58.2</u>	60.5
Layer × Element Mixed	<u>66.0</u>	69.1	62.0	65.7	80.7	94.1	87.4	77.4	<u>70.6</u>	72.5	80.7	71.3	74.5	<u>64.2</u>	60.9	60.5	61.9

Table 8: Full results of the ablation studies on merging coefficient. We report accuracy across all datasets and their average per task group. **Bold** indicates the best and underline indicates the second best.

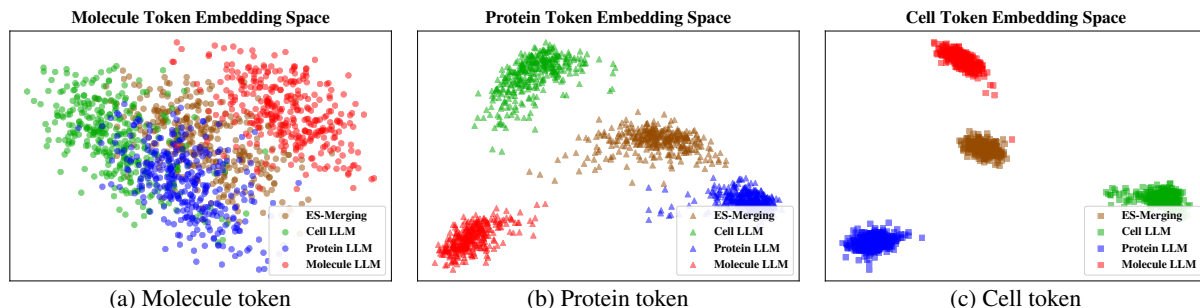


Figure 8: Embedding visualization of the last transformer block for each specialized LLM and the merged model with our method for (a) molecule, (b) protein, and (c) cell tokens.

coefficient distributions are far from uniform, indicating that layer-wise global coefficients alone cannot capture the fine-grained specialization differences and supporting the necessity of element-wise local coefficients.

C.1.3 Final Coefficients of ES-Merging

The layer-wise global coefficient $\alpha_{m_i}^l$ and the element-wise local coefficient $\beta_{m_i}^{l,n}$ focus on different regions. The layer-wise coefficient captures coarse-grained distributional shifts in the embedding space, while the element-wise coefficient reflects fine-grained importance at the individual parameter level. As formulated in Eq. 4, by multiplying these two coefficients and normalizing, regions where both coefficients assign high importance are amplified, whereas regions where only one side is high and the other is low are suppressed. This enables merging that simultaneously incorporates global layer-level specialization signals and local element-level specialization signals. As shown in Figure 10, compared to the element-wise-only coefficient distributions, the combined results demonstrate that the overall scale of coefficients is adjusted according to the global importance of each layer, while the fine-grained element-level patterns are preserved.

C.2 Details of Ablation Study

Table 8 reports the detailed per-dataset results corresponding to the averages of each task group in Table 3. The layer-wise ES-Merging and element-wise ES-Merging each dominate on differ-

ent datasets. Despite this dataset-level variations, Layer×Element ES-Merging consistently achieves the best or comparable performance across all individual datasets. These results confirm that the two coefficients capture specialization at different granularities depending on task and dataset characteristics, and their combination compensates for the weaknesses of either side, yielding consistent and robust merging performance at the individual dataset level as well.

C.3 Embedding Visualization

Figure 8 visualizes the embedding distributions of each specialist model and the model merged by ES-Merging at the last transformer block for each modality token. In each modality token space, the specialist models form distinct distributions, indicating that each model has learned modality-specific representations. The model merged by ES-Merging is positioned between the specialist distributions without being biased toward any particular specialist, while being relatively close to the distribution of the specialist corresponding to each modality token. This suggests that ES-Merging integrates the modality-specific knowledge of each specialist model in a balanced manner, while preserving the specialization for each modality.

D Limitation

In this work, we present ES-Merging, a novel MLLM merging framework that derives layer-wise and element-wise merging coefficients by leveraging embedding space signals. Although we have

demonstrated its effectiveness on the integration of MLLMs specialized in biochemical domains such as molecules, proteins, and single cells, we have not explored its applicability to more general multi-modal domains such as video, image, and audio due to the lack of cross-modal benchmarks on these domains. Since the core principle of our approach to leverage embedding space signals is inherently modality-agnostic, we believe that extending ES-Merging to such general multi-modal scenarios is a promising direction and leave this exploration as future work. Additionally, further investigation is needed to verify whether ES-Merging can maximally preserve performance not only on cross-modal fusion tasks but also on individual single-modality tasks of each specialist model.

Table 9: In-context learning prompt templates for the Molecule-Protein Interaction and CYP prediction task. Angle-bracketed tokens are replaced with the corresponding encoder embeddings: `<protein>` and `<mol>` for the target pair, and `<protein k>` and `<molecule k>` for each of the k few-shot examples. The `<label>` token is replaced with the ground-truth prediction string for each example pair in the few-shot context.

Prompt for Molecule-Protein Interaction Prediction

System

You are an expert specialized in drug discovery and molecular biology. You will be given a protein and a molecule. Your task is to **determine whether a given molecule interacts with a specific protein.**

User

Determine whether the given molecule interacts with the protein by following the examples.

Examples:

Example 1: Protein: `<protein 1>` Molecule: `<molecule 1>` Final answer: {Label}

⋮

Example k : Protein: `<protein k>` Molecule: `<molecule k>` Final answer: {Label}

Protein: `<protein>` Molecule: `<mol>`

Your final answer must be exactly one of: **‘Final answer: Interacts’** or **‘Final answer: Does not interact’**.

Prompt for CYP Inhibition Prediction

System

You are an expert specialized in drug discovery and molecular biology. You will be given a protein and a molecule. Your task is to **determine whether a given molecule inhibits a specific protein.**

User

Determine whether the given molecule inhibits the protein by following the examples.

Examples:

Example 1: Protein: `<protein 1>` Molecule: `<molecule 1>` Final answer: {Label}

⋮

Example k : Protein: `<protein k>` Molecule: `<molecule k>` Final answer: {Label}

Protein: `<protein>` Molecule: `<mol>`

Your final answer must be exactly one of: **‘Final answer: Inhibit’** or **‘Final answer: Does not inhibit’**.

Prompt for CYP Substrate Prediction

System

You are an expert specialized in drug discovery and molecular biology. You will be given a protein and a molecule. Your task is to **determine whether a given molecule is a substrate of a specific protein.**

User

Determine whether the given molecule is a substrate of the protein by following the examples.

Examples:

Example 1: Protein: `<protein 1>` Molecule: `<molecule 1>` Final answer: {Label}

⋮

Example k : Protein: `<protein k>` Molecule: `<molecule k>` Final answer: {Label}

Protein: `<protein>` Molecule: `<mol>`

Your final answer must be exactly one of: **‘Final answer: Substrate’** or **‘Final answer: Not a substrate’**.

Table 10: In-context learning prompt template for the Molecule-Cell Interaction prediction task. Angle-bracketed tokens are replaced as follows: target molecule token `<mol>` and `<molecule k>` for each of the k few-shot examples are substituted with the corresponding encoder embedding, while the gene tokens `<gene>` are replaced with the corresponding cell line string. The `<Label>` token is replaced with the ground-truth prediction string for each example pair in the few-shot context.

Prompt for Molecule-Cell Interaction Prediction: GDSC2

System

You are an expert specialized in cancer pharmacogenomics and drug response prediction. You will be given an anticancer molecule and a cancer cell represented as a list of gene names ordered by expression, where the most highly expressed genes appear first in descending order. Your task is to predict whether the molecule will biologically suppress the cancer cell. **If the molecule is expected to suppress/inhibit cancer cell growth or viability, label it Sensitive, otherwise label it Resistant.**

User

Determine whether the given cell is sensitive or resistant to the given molecule based on the ranked gene-expression list.

Examples:

Example 1: Cell: `<gene 1>` Molecule: `<molecule 1>` Final answer: {Label}

⋮

Example k : Cell: `<gene k>` Molecule: `<molecule k>` Final answer: {Label}

Cell: `<gene>` Molecule: `<mol>`

Your final answer should be formatted as either: **'Final answer: Sensitive'** or **'Final answer: Resistant'**.

Prompt for Molecule-Cell Interaction Prediction: DrugComb

System

You are an expert specialized in cancer pharmacogenomics and anticancer drug-combination response prediction. You will be given two anticancer molecules and a cancer cell represented as a ranked list of gene names (highest expression first). Your task is to predict the binary interaction outcome in terms of anticancer effect in that cell line.

Labels:

Synergistic – the combination produces a stronger anticancer effect than expected,

Antagonistic – the combination produces a weaker anticancer effect than expected.

User

Predict whether the drug pair is Synergistic or Antagonistic in the given cell line.

Examples:

Example 1: Cell: `<gene 1>` Molecule1: `<molecule1 1>` Molecule2: `<molecule2 1>` Final answer: {Label}

⋮

Example k : Cell: `<gene k>` Molecule1: `<molecule k>` Molecule2: `<molecule2 k>` Final answer: {Label}

Cell: `<gene>` Molecule1: `<mol1>` Molecule2: `<mol2>`

Your final answer should be formatted as either: **'Final answer: Synergistic'** or **'Final answer: Antagonistic'**.

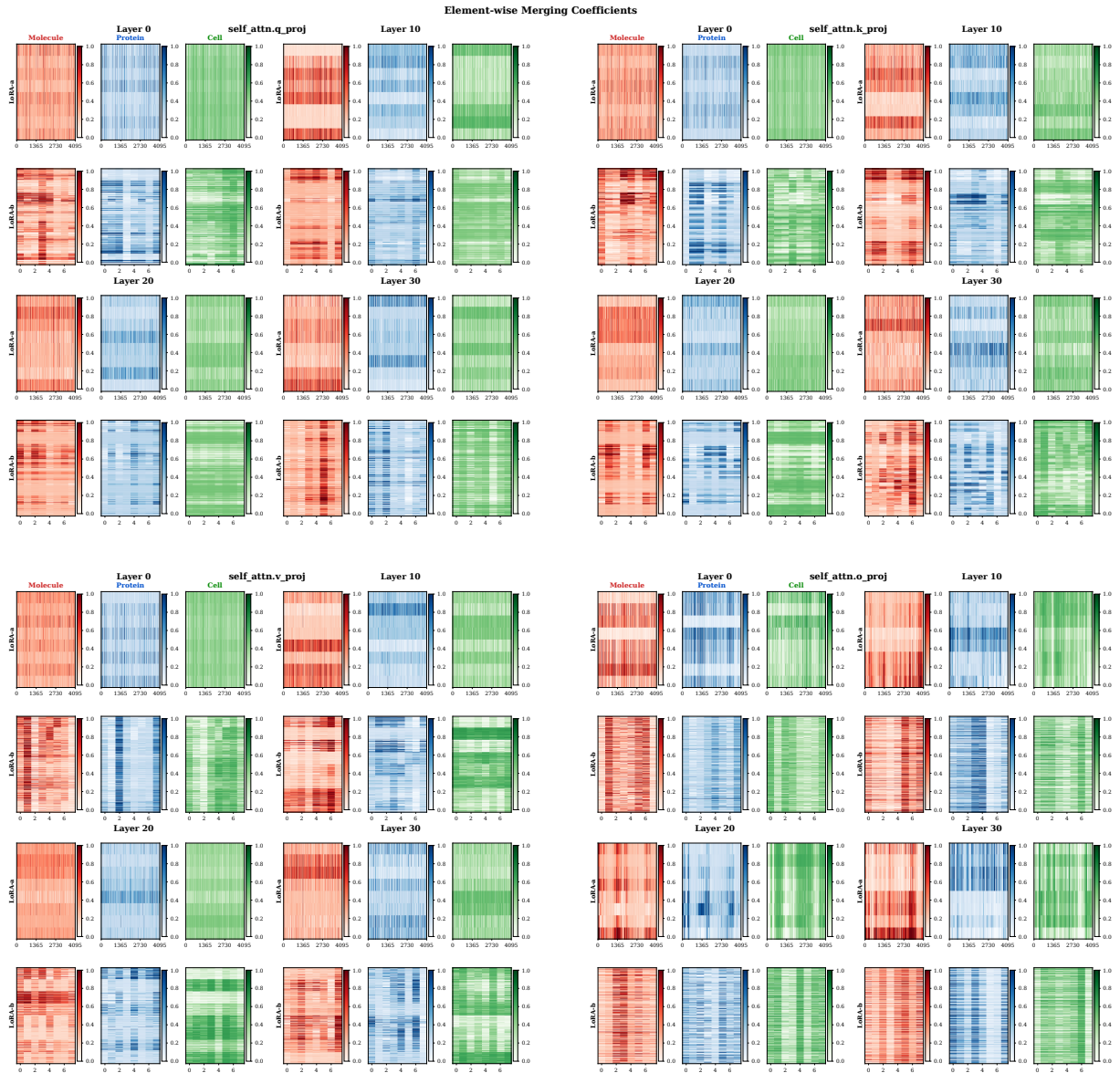
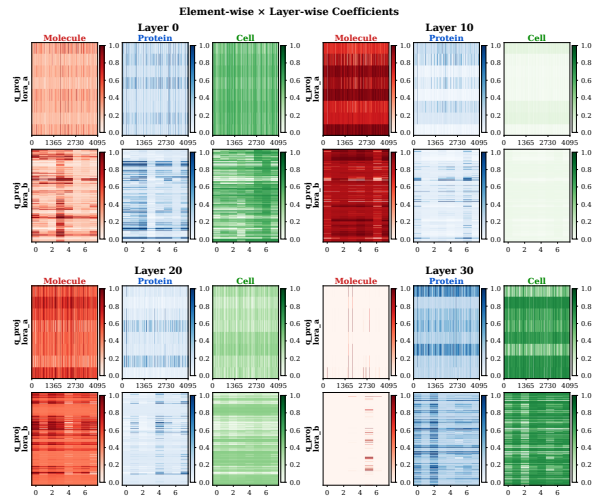
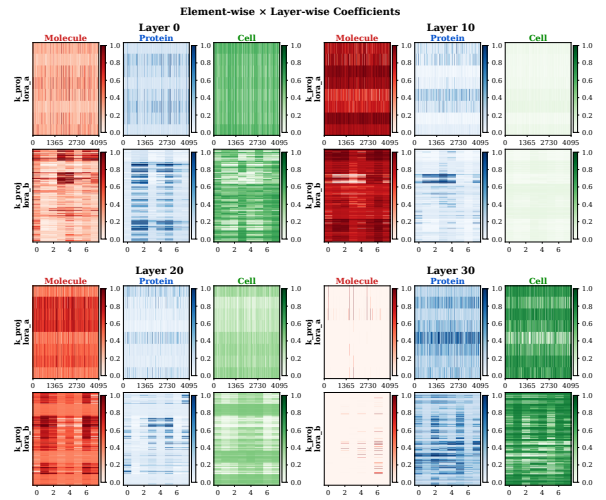


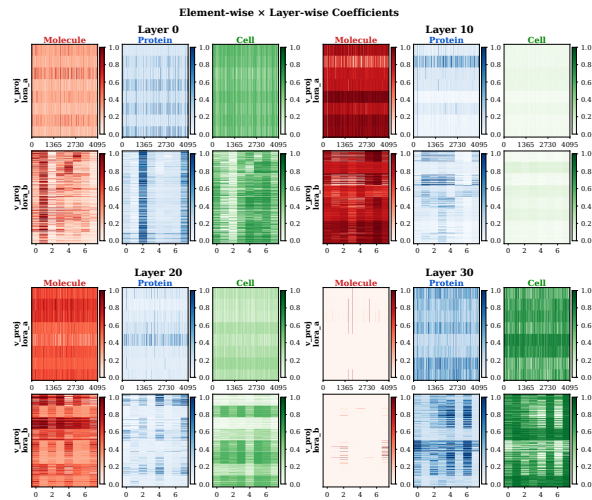
Figure 9: Element-wise merging coefficients of the LoRA parameters for `self_attn.q/k/v/o_proj` modules at layers 0, 10, 20, and 30. Rows correspond to LoRA-A and LoRA-B, and columns correspond to Molecule, Protein, and Cell modalities.



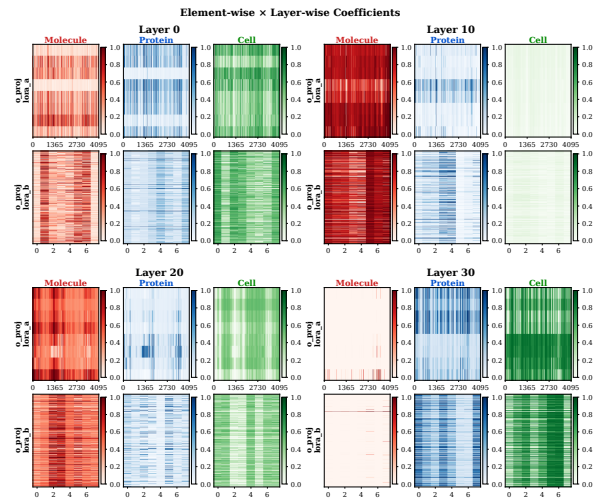
(a) q projection



(b) k projection



(c) v projection



(d) o projection

Figure 10: Element \times Layer merging coefficients of the LoRA parameters for self_attn.q/k/v/o_proj modules at Layers 0, 10, 20, and 30, respectively.